J Gastroenterol (2017) 52:327–340
DOI 10.1007/s00535-016-1222-0

The Japanese Society of Gastroenterology

ORIGINAL ARTICLE—ALIMENTARY TRACT

Aberrant BLM cytoplasmic expression associates with DNA damage stress and hypersensitivity to DNA-damaging agents in colorectal cancer

Carolina Votino[1] · Carmelo Laudanna[2] · Pietro Parcesepe[3] · Guido Giordano[4] · Andrea Remo[5] · Erminia Manfrin[4] · Massimo Pancione[1,6]

Received: 30 October 2015 / Accepted: 26 April 2016 / Published online: 11 May 2016

Abstract
Background Bloom syndrome is a rare and recessive disorder characterized by loss-of-function mutations of the *BLM* gene, which encodes a RecQ 3′–5′ DNA helicase. Despite its putative tumor suppressor function, the contribution of *BLM* to human sporadic colorectal cancer (CRC) remains poorly understood.
Methods The transcriptional regulation mechanism underlying *BLM* and related DNA damage response regulation in independent CRC subsets and a panel of derived cell lines was investigated by bioinformatics analysis, the transcriptomic profile, a CpG island promoter methylation assay, Western blot, and an immunolocalization assay.
Results In silico analysis of gene expression data sets revealed that *BLM* is overexpressed in poorly differentiated CRC and exhibits a close connection with shorter relapse-free survival even after adjustment for prognostic factors and pathways that respond to DNA damage response through ataxia telangiectasia mutated (ATM) signaling. Functional characterization demonstrated that CpG island promoter hypomethylation increases *BLM* expression and associates with cytoplasmic BLM mislocalization and increased DNA damage response both in clinical CRC samples and in derived cancer cell lines. The DNA-damaging agent *S*-adenosylmethionine suppresses *BLM* expression, leading to the inhibition of cell growth following accumulation of DNA damage. In tumor specimens, cytoplasmic accumulation of BLM correlates with DNA damage and γH2AX and phosphorylated ATM foci and predicts long-term progression-free survival in metastatic patients treated with irinotecan.
Conclusions Taken together, the findings of this study provide the first evidence that cancer-linked DNA hypomethylation and cytosolic BLM mislocalization might reflect compromised levels of DNA-repair activity and enhanced hypersensitivity to DNA-damaging agents in CRC patients.

Keywords DNA damage response · DNA repair · Bloom syndrome gene · γH2AX · Phosphorylated ataxia telangiectasia mutated · CpG island promoter hypomethylation

C. Votino, C. Laudanna, and P. Parcesepe are joint first authors.

Electronic supplementary material The online version of this article (doi:10.1007/s00535-016-1222-0) contains supplementary material, which is available to authorized users.

✉ Massimo Pancione
massimo.pancione@unisannio.it

1 Department of Sciences and Technologies, University of Sannio, Via Port'Arsa, 11, 82100 Benevento, Italy

2 Department of Experimental and Clinical Medicine "Gaetano Salvatore", University "Magna Grecia", 88100 Catanzaro, Italy

3 Department of Surgery and Oncology, University of Verona, 37129 Verona, Italy

4 Medical Oncology Unit, Fatebenefratelli Hospital, 82100 Benevento, Italy

5 Department of Pathology, "Mater Salutis" Hospital, 37045 Legnago, VR, Italy

6 Department of Biochemistry and Molecular Biology, Faculty of Pharmacy, Complutense University, Madrid, Spain

Background

Genomic instability is a characteristic of almost all human cancers, the molecular basis of which is still uncertain [1–3]. Bloom syndrome is a rare autosomal recessive disorder

that predisposes to chromosomal instability and a high incidence of tumors, including colorectal cancer (CRC) [4–6]. It is caused by mutations in the *BLM* gene, deficiency of which results in excessive chromosomal breakage, hyper-recombination due to a high rate of sister chromatid exchange, and locus-specific mutations [1, 4–6]. Despite the close connection between Bloom syndrome and chromosomal instability, *BLM*-deficient cells display a diploid karyotype, in stark contrast to non-Bloom syndrome adenomas, which generally show chromosomal gains/losses even at an early stage [7, 8]. Defects in the DNA damage response (DDR) process, aberrant DNA replication timing, and replication stress have been associated with changes in gene expression, epigenetic modifications, and an increased frequency of chromosomal structural rearrangements [9–13]. Recent studies have demonstrated that chromosomal instability can be a consequence of increased levels of replication-dependent double-strand breaks [9–11]. In addition to *BLM*, germline mutations of two other RecQ helicases, *WRN* in Werner syndrome and *RECQL4* in Rothmund–Thomson syndrome, are also associated with an elevated incidence of cancers [6–10]. The *WRN* gene has been found inactivated because of promoter methylation in different cancer types, regardless of CpG island methylator phenotype (CIMP) and microsatellite instability status [14]. Similarly, other DNA repair family tumor-suppressor genes such as *MLH1*, *MGMT* and *BRCA1* have been described undergoing epigenetic inactivation by promoter hypermethylation [14]. Given that *BLM* is rarely mutated in sporadic tumors, in this work we aimed to identify additional alterations that characterize *BLM* in sporadic CRC. We here show that *BLM* undergoes CpG island promoter hypomethylation, a mechanism that increases its expression, resulting in a cytoplasmic mislocalization and increased levels of DNA damage. We provide evidence that overexpression of *BLM* is associated with high-grade tumors and shorter relapse-free survival in patients. The results presented here could help to identify patients who have higher chances of benefiting from specific chemotherapeutic agents that target the DDR pathway.

Materials and methods

Gene expression analysis in public CRC data sets

Genome-wide messenger RNA (mRNA) expression data available from four public data sets were used as discovery sets by application of in silico bioinformatics analysis. The following series were analyzed: (1) the Cancer Genome Atlas series of 210 patients (cohort I); (2) the GSE41258 series of 146 patients (cohort II); (3) the GSE17536/GSE17537 pooled series of 226 patients (cohort III); (4) the Cancer Cell Line Encyclopedia, Broad Institute/Novartis series comprising 60 CRC cell lines [15–18]. The Cancer Genome Atlas series (cohort I), although it was obtained with a non-Affymetrix platform, allows us to investigate matched tumor and normal samples ($n = 20$), extensive tumor-related DNA alteration annotations (whole-exome sequencing, copy number alterations, DNA methylation profiles), and patients' survival follow-up data (Fig. S1). Tumors were defined on the basis of the weighted genome instability index either as chromosomal instability positive (more than 0.2 copy number alterations) or as chromosomal instability negative (0.2 or fewer copy number alterations). The differentially expressed genes between tumor and normal samples were quantified by application of RSEM ratio levels. Statistical evaluation was performed by a paired *t* test. The GSE41258 and GSE17536/GSE17537 data sets fulfilled the following criteria: available genome-wide mRNA expression analysis data obtained with a similar chip platform (Affymetrix U133 Plus 2.0 chips) and complete disease specific survival data. In addition, within cohort III, there were 220 patients with documented relapse (distant and/or locoregional recurrence) available for recurrence analysis. Genes showing altered expression (false discovery rate $q < 0.05$) were ranked according to the degree of expression difference in each data set. Volcano plot analysis was used to visualize the differential gene expression in data sets without matched normal references. Supervised analysis of differentially expressed gene profiles was first filtered for absolute fold change of 1.5 or greater. Statistical analysis was performed with use of Student's *t* test ($p \leq 0.05$). Gene Ontology and KEGG pathway enrichment analysis of the resulting differentially expressed genes was conducted with use of the Database for Annotation, Visualization and Integrated Discovery (DAVID) (https://david.ncifcrf.gov/). The investigation of potential *BLM* molecular networks and canonical pathways was performed with Ingenuity Pathway Analysis from Ingenuity Systems (http://www.ingenuity.com). Statistical analyses were performed by GeneSpring R/bioconductor version 12.5.

Patients and tissues

Two hundred thirty-two patients with sporadic CRC who had undergone routine surgery were recruited from two community hospitals—the Department of Pathology and Oncology, Legnago Hospital, Verona, Italy, and the Department of Surgery and Oncology, University of Verona, Verona, Italy—between January 2003 and December 2010. The entire population study consisted of two independent cohorts: (1) a training cohort of 130 formalin-fixed, paraffin-embedded tumor samples, 82 of which

included sections of fresh tissue specimens from tumor and matched normal adjacent mucosa frozen in liquid nitrogen and stored at −80 °C until RNA isolation (available clinicopathology data for this series are summarized in Table S1); (2) a validation series consisting of 102 metastatic CRC patients (54 men and 48 women) receiving irinotecan with folinic acid and 5-fluorouracil chemotherapy-based schedules. The clinical follow-up data included (1) patients' overall survival, defined as the time elapsed between the start of first-line chemotherapy and death, and (2) progression-free survival, defined as the time elapsed between the start of first-line chemotherapy and disease progression, treatment discontinuation, or death. For both series, tumor stage was determined according to guidelines from the International Union Against Cancer/American Joint Committee on Cancer. Microsatellite instability status as well as other molecular parameters of tumor differentiation including *TP53* and CIMP status have already been reported for training series [19, 20]. For details about both data sets, the complete workflow of the study is summarized in Fig. S1.

All the samples were routinely fixed in 10 % formalin, embedded in paraffin, sectioned consecutively at 4 µm, and stained by hematoxylin and eosin to assign the histologic types. A group of formalin-fixed, paraffin-embedded samples of apparently normal mucosa samples ($n = 60$) isolated during the same surgery served as internal controls. None of the patients had received adjuvant chemotherapy or radiotherapy. All patients gave informed consent for sample collection and molecular analyses, and study protocols were in accordance with the ethical guidelines of the Declaration of Helsinki and were approved by the institutional review boards of the hospitals.

Tissue microarrays, immunohistochemistry, and evaluation of immunostaining

Tissue microarrays (TMAs) were constructed from tissue blocks of normal colon tissue and CRC as previously reported [19]. Briefly, 4-µm-thick sections were cut from each TMA block and sections were then reviewed to ensure that those from each case were morphologically similar to those of the corresponding whole tissue section and represented cancerous or normal epithelial cells. For immunohistochemistry evaluation, 232 CRCs and 60 normal colon tissues were available. Immunohistochemistry assays were initially performed on representative whole tissue sections by our evaluating the overall concordance between tissue specimens and paired TMA cores. TMAs were used to evaluate marker expression in the validation data sets. The TMAs were serially sectioned at 4 µm, dewaxed in xylene, and rehydrated through graded alcohol to water. Slides were subjected to microwave antigen retrieval in 10 mM citrate buffer (pH of 6.0) before incubation with the primary antibodies. A rabbit monoclonal antibody against BLM (1:50, clone H-300, Santa Cruz Biotechnology, Denmark) was incubated overnight at 4 °C. The secondary antibody and then a streptavidin–horseradish system were incubated for 30 min each, by use of a streptavidin–biotin peroxidase staining kit (LSAB+System-HRP; Dako Cytomation, Glostrup, Denmark). Immunoreactivity was revealed by incubation in 3,3-diaminobenzidine substrate for 5 min. Subsequently, the sections were counterstained with hematoxylin, dehydrated, and cover with a coverslip. Primary antibodies were omitted in negative controls. For each core section, at least 500 cells were examined. BLM immmunostaining was evaluated by assigning no cutoff value, regardless of intensity and taking into account the distribution of the positivity in the cytoplasmatic and/or nuclear compartment as follows: (1) subcellular cytoplasmic expression (*C*) was defined as the presence of a homogeneous cytoplasmic staining in more than 50 % of tumor cells; (2) nuclear immunoreactivity (*N*) corresponded to a homogeneous nuclear staining in more than 50 % of tumor cells; (3) cytoplasmic/nuclear immunostaining (*N*/*C*) exhibited a mixture of nuclear and cytoplasmic immunohistochemical positivity. Nuclear immunoreactivity for γH2AX and phosphorylated ataxia telangiectasia mutated (pATM) was classified into two patterns: (1) focal "characterized by focus formation" in a limited number of tumor cells scattered in a background of either negative or weakly positive tumor cells; (2) diffuse staining "covering the entire nucleus" in more than 50 % of tumor cells as previously reported [21]. All immunohistochemistry results were interpreted by two independent observers (A.R. and M.P.) blinded to the clinical data.

CRC cell lines and DNA methylation analysis

The human CRC-derived cell lines HT29, CaCo-2, Geo, SW480, RKO, LoVo, and DLD1 were purchased from American Type Culture Collection (Rockville, MD, USA). All cell lines were maintained in Dulbecco's modified Eagle's medium or RPMI 1640 medium supplemented with 10 % fetal bovine serum, 2 mM L-glutamine, penicillin, and streptomycin. Cells were cultured in a humidified 37 °C incubator at 5 % CO_2. Additionally, wild-type HCT116 cells and HCT116 cells with the DNA methyltransferases DNMT1 and DNMT3b knocked out were investigated [22].

Genomic DNA was isolated from cells and tissues, and bisulfite modification and methylation-specific PCR (MSP) primers were designed following procedures already described [23]. For all MSP experiments, each plate

included an unmethylated control (bisulfite-treated normal leukocyte DNA) and a methylated control (bisulfite-converted in vitro methylated human DNA; Chemicon, Millipore).

Bisulfite cloning sequencing was conducted on selected PCR amplification products to confirm the reliability of the MSP assays. Primer sequences and PCR conditions are reported in Table S2. The methylation levels (ratio of methylated to unmethylated and methylated DNA) were determined from the relative band intensities. Methylation levels greater than 15 % were considered positive, consistent with the threshold used in other studies [14]. To gain further insight into CpG island methylation levels of primary CRC and matched normal colon tissues, we used the publicly available data set GSE39068 analyzed by comprehensive genome-wide DNA methylation profiles. This cohort comprised 24 patients, of whom 22 were also included in the present study, making possible the association between methylated CpG density and expression profiles. Methylation data for each sample were calculated as the number of reads overlapping each region of interest and were normalized by division by the total number of aligned reads of the sample, and the length of the peak, as described before [22].

Messenger RNA extraction and quantitative real-time reverse transcription PCR analysis and Western blot analysis

Total RNA was purified from CRC cell lines and clinical specimens by use of the reported procedure. SuperScript II and random hexamer primers (Invitrogen, San Diego, CA, USA) were used for reverse transcription PCR (RT-PCR). The resulting complementary DNA was PCR amplified to detect the specific mRNAs of interest, with normalization against the housekeeping gene 18S. The amplified products were run on a 3 % agarose gel, stained with ethidium bromide, and visualized under a UV transilluminator. To get quantitative results of the mRNA levels, quantitative real-time RT-PCRs were performed in triplicate with a 7300 real-time PCR system (Applied Biosystems, Foster City, CA, USA) with sue of SYBR Green PCR master mix and 200 ng of template complementary DNA. The primers and conditions for RT-PCR analysis are reported in Table S3. Western blot analysis on total protein extracts was performed as previously reported [23]. The primary antibodies used were as follows: anti-BLM (H-300, diluted 1:250, Santa Cruz Biotechnology), anti-γH2AX (phosphorylated Ser139, diluted 1:5000, Abcam), anti-pATM (phosphorylated Ser1981, diluted 1:1000, Abcam), anti-vimentin (ab137321, diluted 1:2000, Abcam), anti-cytokeratin 20 (H-70, diluted 1:500), and anti-retinoic acid receptor β (C-19, diluted 1:200, Santa Cruz Biotechnology). Nuclear and cytoplasmic fractions for Western blot analysis were obtained by use of an NE-PER extraction kit (Thermo Scientific). Purity of fractions was proven with two different nuclear and cytoplasmic markers: anti-histone H3 (FL-136, diluted 1:500, Santa Cruz Biotechnology) and anti-β-actin, (diluted 1:1000, Sigma-Aldrich Milan, Italy). Image acquisition and densitometric analyses were performed with a ChemiDoc XRS imaging system (Bio-Rad, Richmond, CA, USA).

Drugs and cell proliferation, and wound-healing analysis

The DNA demethylating agent 5-aza-2′-deoxycytidine (Sigma, St Louis, MO, USA) was administered at 1 or 5 μM for 72 h. The growth medium with 5-aza-2′-deoxycytidine was changed every 24 h. The DNA methylating agent *S*-adenosyl-L-methionine (SAM) was administered at 250 μM for 72 h as was its unmethylated analogue *S*-adenosyl-L-homocysteine. After the treatments, cells were harvested for RNA extraction. Cell migration was evaluated by a wound-healing assay. A proliferation assay and cell cycle analysis were performed with use of propidium iodide staining as previously reported [23].

Silencing of *BLM* expression

DLD1 cells were seeded in six-well plates and transfected transiently with Lipofectamine 3000 (Invitrogen) according to the manufacturer's recommendations with a pool of short hairpin RNA (shRNA) plasmid specific for BLM (sc-29808-SH) or control short hairpin RNA expression plasmid (sc-108060) and selected in puromycin for 1 week (Santa Cruz Biotechnology). In both cases, derived colonies were amplified and harvested for protein extraction and for efficient *BLM* silencing. Cytomorphologic analysis of cultured cells at early and late passages was performed by hematoxylin–eosin staining as previously reported [23]. Cells were incubated complete Dulbecco's modified Eagle's medium and then treated with the demethylating agent 5-aza-2′-deoxycytidine at 1 μM and the methylating agent SAM at 250 μM and its unmethylated analogue *S*-adenosyl-L-homocysteine at different times. A proliferation assay and cell cycle analysis were performed with use of propidium iodide staining. The colorimetric substrate was measured and quantified at 560 nm in an enzyme-linked immunosorbent assay plate reader.

Immunofluorescence analysis

About 100,000 cells were plated on coverslips; after 24 h, they were washed twice in phosphate-buffered saline and fixed with 4 % paraformaldehyde in phosphate-buffered

saline for 10 min at room temperature. Blocking was performed with 3 % bovine serum albumin, and the primary antibodies employed were as follows: anti-BLM diluted 1:50; anti-γH2AX diluted 1:500, and anti-pATM diluted 1:500. They were incubated for 30 min at room temperature. Fluorescently conjugated secondary antibody tetramethylrhodamine-5-(and 6)-isothiocyanate was used to visualize the reaction. Finally, 4′,6-diamidino-2-phenylindole staining was performed and, after three washes in cold phosphate-buffered saline, coverslips were mounted in Mowiol 4-88 (Calbiochem, CA, San Diego, USA) on glass slides. Image acquisition and analysis were performed with a Nikon Eclipse E600 system (PA, USA).

Statistics

The distributions of BLM mRNA and protein were characterized by their median values and ranges. Relationships between BLM mRNA and protein levels and between BLM mRNA and protein levels and clinical parameters were identified by means of Pearson rank correlation and nonparametric Kruskal–Wallis or Wilcoxon–Mann–Whitney tests. The percentages of cells with three or more γH2AX and pATM foci ($n > 100$ per cell line) were compared by the Mann–Whitney U test. Groups of means were compared by analysis of variance and Student's t test. The Kaplan–Meier method was used to estimate survival; the log-rank test was used to test differences between the survival curves. Prognostic effects were assessed with use of three clinical end points: overall survival, progression-free survival, and relapse-free survival. The Cox proportional hazards model was used to estimate hazard ratios (HRs) with 95 % confidence intervals (CIs). Multivariate models were adopted with adjustment for factors known to be prognostic in CRC. Statistical analyses were conducted with R statistical software, SPSS version 15 for Windows (SPSS, Chicago, IL, USA), and GraphPad Prism 5. Data are presented as medians and ranges where indicated. $P \leq 0.05$ was considered statistically significant.

Results

Upregulation of *BLM* correlates with the ataxia telangiectasia mutated signaling pathway in sporadic CRC

To investigate whether *BLM* mRNA expression level is associated with clinical disease progression in CRC, we first interrogated the Cancer Genome Atlas data set of 210 samples, named cohort I, for which 21 nonneoplastic mucosas were available (Fig. S1). *BLM* mRNA showed higher expression in tumor tissues than in nonneoplastic mucosa, whereas no significant differences emerged when tumors were stratified according to common clinicopathologic factors ($P = 0.0003$; Figs. 1a, S2a–c). To define the relationship between *BLM* expression levels and molecular parameters of the tumors, we evaluated CIMP and DNA mismatch repair. To this end, CRCs with *BLM* mRNA expression above the median value relative to normal mucosa were classified as having high *BLM* expression, and the rest were classified having low *BLM* expression. The percentage of tumors expressing high *BLM* mRNA levels was greater in CIMP tumors than in non-CIMP tumors, and accordingly mismatch-repair-positive tumors tend to have a greater frequency of high *BLM* expression than mismatch-repair-negative tumors (62% vs 37 % and 66 % vs 34 % respectively, $P < 0.05$; Fig. S2d). In light of biological alterations that characterize Bloom syndrome, the upregulation of *BLM* appears to be relevant and piqued our further interest. Notably, genomic data did not provide a genetic explanation for *BLM* upregulation, with a lack of copy number alterations and loss of heterozygosity at the *BLM* locus ($P = 0.35$; Fig. 1b). Transcriptomic profiling revealed a higher number of BLM co-upregulated genes than downregulated genes (3412 of 4063, 84 %, vs 651 of 4063, 16 %; $P = 0.0001$) and significant enrichments for BLM-overexpressing tumors related to malignant transformation and cellular response to DNA damage mainly involving ataxia telangiectasia mutated (ATM) and H2AX signaling regardless of *TP53* status (Figs. 1c, d, S2d, Table S3). Analysis of two additional independent data sets, cohorts II and III, provided further support for the overexpression of BLM and related pathways. Volcano plots confirmed that *BLM* mRNA is frequently upregulated in tumors, as more than 50 % of cases were included above the median value ($P < 0.05$; Fig. 2a). In silico findings from these cohorts supported the role of DNA damage checkpoint, cytoplasmic functions, and a mitotic process through ATM signallng in *BLM*-upregulated tumors, whereas the cluster of "downeegulated genes," characterized protein binding, intercellular communication signals, and cell adhesion pathways (Fig. S3). Notably, a significantly higher proportion of poorly differentiated CRCs, as opposed to moderately or well-differentiated carcinomas, showed higher BLM expression, supporting its role in a distinct subgroup of CRCs for which responses to treatment differ from those of patients with prototypical adenocarcinoma ($P = 0.002$, Fig. 2b) [17].

We next assessed the impact of variations of *BLM* mRNA levels on patient outcome by studying survival curves. Tumors expressing high *BLM* levels compared with those with low *BLM* mRNA expression were not associated with patients' overall survival (Fig. S4). Notably, when we explored the association with disease recurrence after surgery

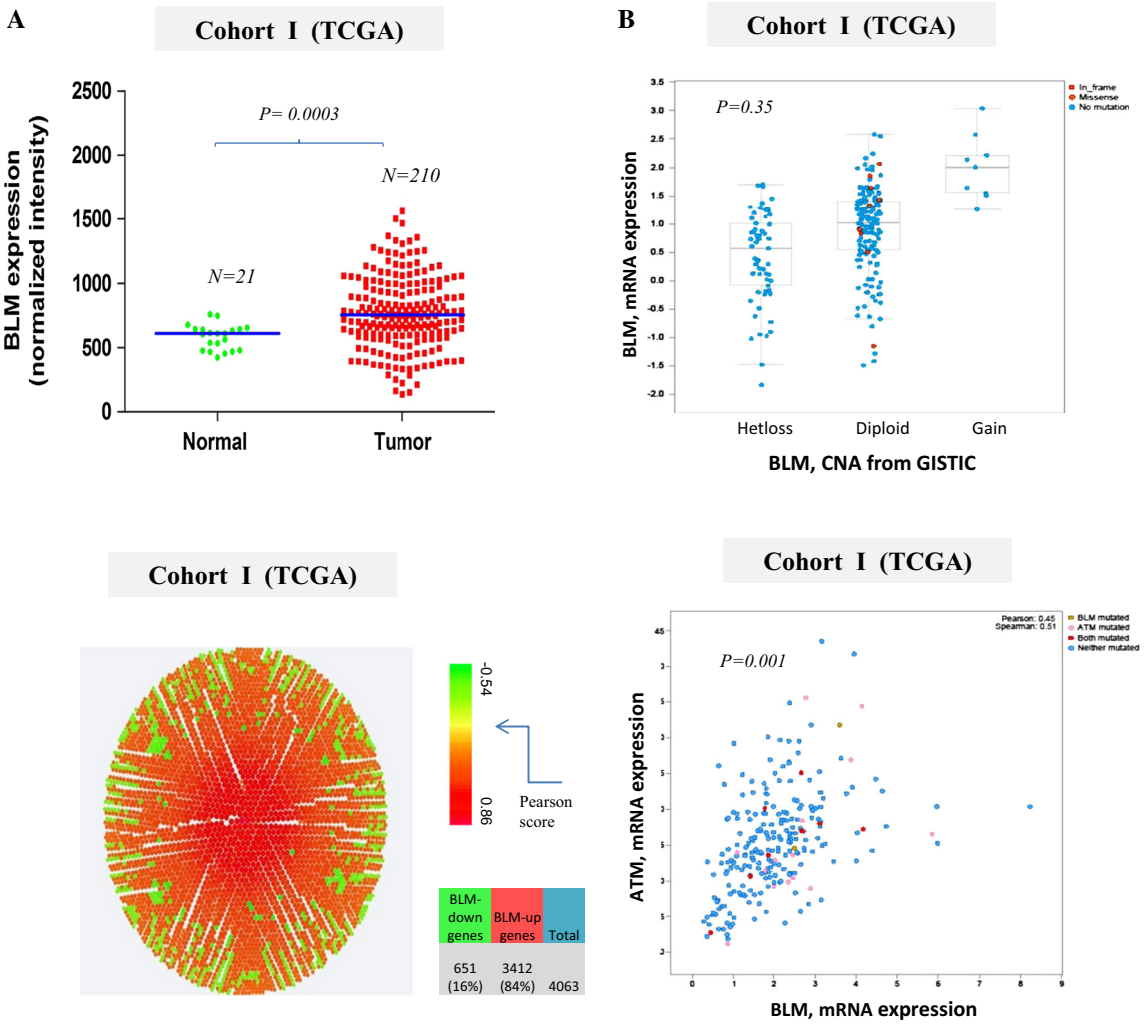

Fig. 1 *BLM* overexpression lacks of genetic alterations and correlates with DNA damage response in the Cancer Genome Atlas (*TCGA*) colorectal cancer data set. **a** Analysis of the *BLM* transcript (RNA sequencing transcriptomic data) in colorectal cancer (cohort I, TCGA data set) using patient-matched tumor–normal samples/"normal intestinal epithelium tissues"). *P* was obtained by Student's *t* test. **b** Lack of mutations and copy number alterations (*CNA*) in relation to *BLM* overexpression at the *BLM* locus. *P* was obtained by the Kruskal–Wallis test. **c** Genome-wide transcription profile shown by the circular density map of the genes significantly coexpressed with *BLM* (for details, see Table S4). *Green* indicates the genes negatively correlated to and *red* indicates those positively correlated to *BLM* transcript by use of Pearson's score ($P > 0.01$). **d** Direct correlation between *BLM* and *ATM* messenger RNA (*mRNA*) expression. *P* was obtained by Pearson's test. *GISTIC*

in cohort III, for which follow-up data were available, we found that high-*BLM*-expression tumors (115 of 226, 51 %) had a significantly shorter recurrence time after surgical resection compared with tumors with low-*BLM*-expression, (Fig. 2c; HR 1.84; 95 % CI 1.01–3.34; $P = 0.044$). Multivariate analysis using a Cox proportional hazards model indicated that a high *BLM* mRNA level was associated with an inferior response to treatment even after adjustment for age, sex, or tumor stage (Fig. 2d; adjusted HR 2.03; 95 % CI 1.10–3.64; $P = 0.023$). These results indicate that overexpression of *BLM* is typically not caused by somatic structural or sequence variations and correlates with ATM signaling pathways and recurrence in CRC patients.

Overexpression of *BLM* leads to cytosolic localization of BLM and increased levels of DDR in CRC cell lines

To examine the mechanisms underlying overexpression of *BLM*, we first examined 82 CRCs and matched normal mucosas from our cohort of patients. CRC samples exhibited higher *BLM* transcript levels than matched normal controls. Likewise *BLM*, as well as its transcript, was upregulated more in tumors than in normal mucosa (Fig. S5a, b). *BLM* mRNA expression was significantly higher in CIMP tumors than in non-CIMP tumors, whereas no significant relationship with microsatellite instability or

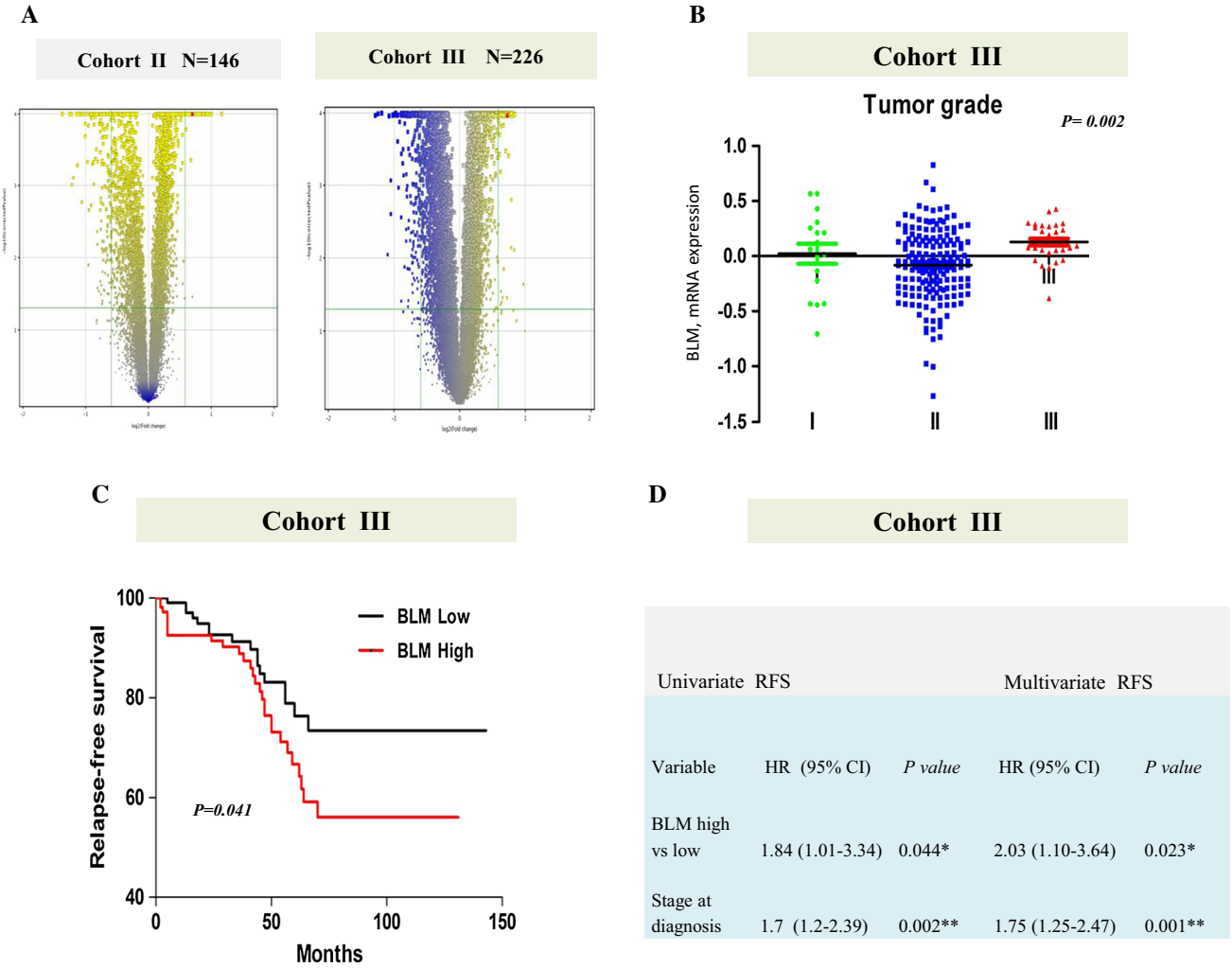

Univariate RFS			Multivariate RFS	
Variable	HR (95% CI)	*P value*	HR (95% CI)	*P value*
BLM high vs low	1.84 (1.01-3.34)	0.044*	2.03 (1.10-3.64)	0.023*
Stage at diagnosis	1.7 (1.2-2.39)	0.002**	1.75 (1.25-2.47)	0.001**

Fig. 2 *BLM* overexpression correlates with histologic differentiation and disease recurrence in independent colorectal cancer data sets. **a** Volcano plot analysis of *BLM* messenger RNA (*mRNA*) expression data in colorectal cancers from cohort II (GSE41258) and cohort III (GSE17536/GSE17537). The *x*-axis is the base 2 logarithm of the fold change, and the *y*-axis is the negative base 2 logarithm of the *q* value (or adjusted *P* value). Thresholds for both the statistical significance ($q < 0.05$) and the biological significance are highlighted and assembled in the *top left corner* and *top right corner* of the graph. **b** Histologic differentiation of the tumors according to *BLM* mRNA expression levels. *P* was obtained by the Kruskal–Wallis test. **c** Relapse-free survival (*RFS*) curve according to *BLM* transcript levels. *P* was obtained by the log-rank test. **d** Cox univariate and multivariate analysis in relation to RFS and adjusted for the stage at diagnosis. *CI* confidence interval, *HR* hazard ratio, $*P \leq 0.05$, $**P \leq 0.01$

TP53 status was observed. (Fig. 5c, d). Consistent with these findings, in silico analysis of 60 CRC cell lines indicated a high frequency of *BLM* mRNA overexpression as compared with those with low expression (38 % vs 16 %, $P = 0.001$). Notably, high *BLM* mRNA expression correlated with molecular subtypes displaying chromosomal instability and CIMP in comparison with low-*BLM*-expression CRC cell lines (70 % and 53 % vs 41 % and 20 % respectively, $P < 0.001$, Fig. 6a, b).

Quantitative RT-PCR analysis from our series of CRC cell lines also confirmed a higher *BLM* transcript level than in normal colon mucosa control specimens taken from healthy donors (Fig. 3a, b). Two CIMP-positive CRC cell lines, DLD1 and RKO, showed a significant overexpression of *BLM*, and were chosen for further study in comparison with the HT29 cell line, in which the levels of *BLM* were relatively low (Fig. 3b). In all three cell lines, *BLM* mRNA levels paralleled protein levels (Fig. 3b). To prove that these variations reflected changes in BLM subcellular localization, we performed immunofluorescence and Western blot analysis. Unexpectedly, we detected a weak but consistent staining in the nucleus of HT29 cells, whereas it was localized mostly in the cytosol or distributed between the cytosol and the nucleus in RKO and DLD1 cells respectively (Fig. 3c). Quantitative Western blot analysis performed on nuclear and cytoplasmic

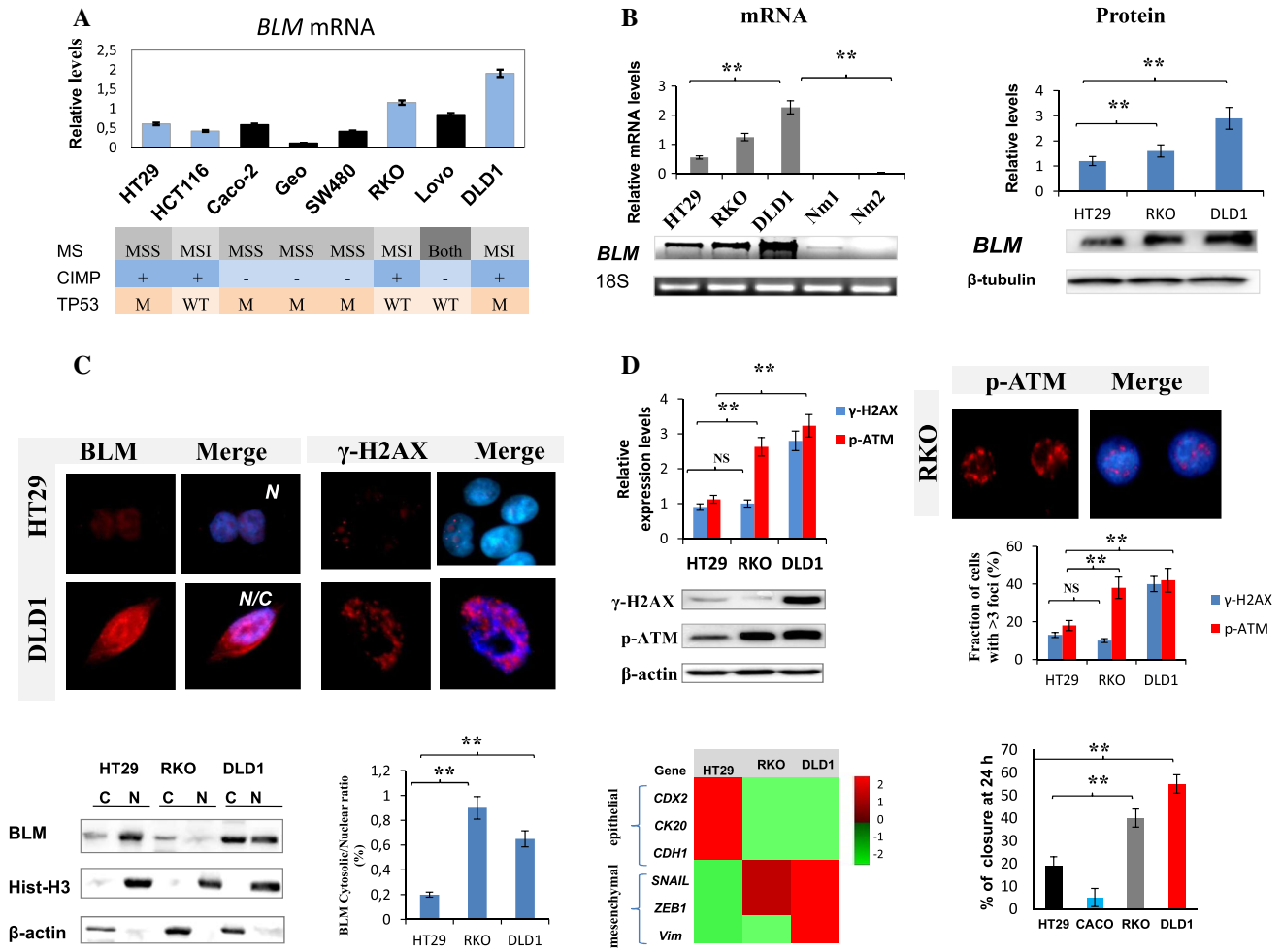

Fig. 3 *BLM* overexpression and cytosolic localization of BLM correlate with increased levels of DNA damage in colorectal cancer (CRC)-derived cell lines. **a** Quantitative reverse transcription PCR (RT-PCR) of *BLM* messenger RNA (*mRNA*) expression according to molecular features of the indicated CRC cell lines. **b** Semiquantitative expression of *BLM* transcript normalized to 18S RNA and Western blot analysis in three representative CRC cells. Two independent normal colorectal mucosa specimens, Nm1 and Nm2 respectively from health donors, were used as controls in RT–PCR analysis. Protein expression levels were normalized to that of β-tubulin. $^{**}P \leq 0.01$ by Student's *t* test. **c** BLM and γH2AX were detected in the CRC cell lines indicated by immunofluorescence analysis. The distribution of γH2AX nuclear foci is compared with BLM subcellular localization. BLM localizes mostly to the nucleus or to both the cytoplasm and the nucleus in HT29 and DLD1 cells respectively. The high cytoplasmic-to-nuclear ratio detected by Western blot analysis on nuclear and cytosolic fractions supports the differential subcellular distribution of BLM in RKO and DLD1 cells. Nuclear and cytoplasmic fractions are validated by histone H3 (*Hist-H3*) and β-actin bands respectively. $^{**}P \leq 0.01$ by Student's *t* test. **d** Western blot analysis shows γH2AX and phosphorylated ataxia telangiectasia mutated (*p-ATM*) expression in HT29, RKO, and DLD1 cells. The percentage of cells ($n > 100$ per cell line) with more than three γH2AX or p-ATM foci is shown. $^{**}P \leq 0.01$, two-tailed *t* test relative to HT29 cells. Quantitative RT-PCR expression (using $\log_2$ fold change) of epithelial and mesenchymal markers for each cell line is indicated. The quantitative RT-PCR data are plotted relative to the housekeeping gene 18S. A wound healing assay at 24 h indicates that cell migration is significantly higher in RKO and DLD1 cells relative to HT29 cells. Data are presented as the mean ± standard deviation of at least three independent experiments. $^{**}P \leq 0.01$ by a two-tailed *t* test. *CIMP* CpG island methylator phenotype, *M* mutated, *MS* microsatellite instability status, *NS* not significant

fractions confirmed the predominant cytoplasmic localizations of BLM in RKO and DLD1 cells, respectively (Fig. 3d). We then investigated whether cytosolic accumulation of BLM correlated with DDR by assessing phosphorylated H2AX (Ser139, γH2AX) and pATM(-Ser1981), which generally mark DNA double-strand breaks [8–10]. In DLD1 cells as compared with HT29 cells, we observed a striking threefold increase of γH2AX and pATM expression levels and increased numbers of relative foci per cell. Consistently, we also observed higher pATM expression in RKO cells than in HT29 cells, further supported by higher numbers of pATM foci per cell but not higher numbers of γH2AX foci per cell ($P > 0.01$; Fig. 3d). In addition to increased DDR, RKO cells and

particularly DLD1 cells showed molecular features of epithelial–mesenchymal transition and enhanced cell migration as compared with HT29 cells ($P > 0.01$; Fig. 3d). These findings indicate that overexpression of *BLM* and cytoplasmic localization of BLM reflects increased levels of DNA damage in representative CRC cell lines.

BLM CpG island promoter hypomethylation leads to gene activation in CRC cell lines

Because *BLM* overexpression associated with CIMP and inspection of the promoter region of *BLM* revealed a canonical 5′-CpG island located around the transcription start site, we hypothesized a methylation-associated regulation in human cancer (Fig. 4a). To analyze the methylation status of the promoter-associated CpG island, we screened eight CRC cell lines by MSP at two promoter regions: region A from −102 to +25 overlapping the transcription start site; region B from −175 to −16, located just upstream of the transcription start site (Fig. 4a). We found that region A was methylated in HCT116 cells alone. In contrast, region B was methylated in HT29, Caco-2, and SW480 cells and correlated with relative lack of *BLM* transcript. Concomitant loss of methylation in either promoter segment correlated with *BLM* overexpressing cells (LoVo, RKO, and DLD1 cells) (Fig. 4b). Bisulfite sequencing confirmed the methylation results obtained by MSP on CRC cell lines and normal controls. We observed methylated CpG residues in the central CpG island of methylated cell lines (CaCo-2 and HT29) and normal colonic mucosa samples (approximately 50 %, Figs. 4b, S7a). In contrast, the unmethylated cell lines RKO and DLD1 showed a lower density of methylation at the *BLM* locus on average, from 8 to 16 % (Figs. 4b, S7a). Promoter hypomethylation and increased *BLM* expression were associated with lower expression of the differentiation markers cytokeratin 20 and retinoic acid receptor β (Fig. S8a). In addition, the DKO cell line, the isogenic partner of the HCT116 cell line with global loss of methylation, showed lack of methylation in the central CpG island at the *BLM* promoter (Fig. S7b). Notably, *BLM* expression was 1.67-fold higher in DKO cells than in wild-type HCT116 cells, supporting the role of DNA methyltransferases to establish locus-specific DNA methylation patterns (Fig. S7b). To further verify whether *BLM* transcript can be regulated by pharmacologic demethylation, HCT116 and Caco-2 cells methylated in regions A and B respectively were exposed to 1 and 5 μM 5-aza-2′-deoxycytidine, a methyltransferase inhibitor. As shown in Fig. 4c, 5-aza-2′-deoxycytidine treatment led to an increased dose-dependent expression of *BLM* mRNA. In parallel, upregulation of *BLM* was associated with lack of methylation in both promoter region A and promoter region B (Fig. 4c). As expected, no variations in fully unmethylated cells (DLD1 cells) on 5-aza-2′-deoxycytidine treatment were observed. By contrast, both mRNA and protein expression levels of BLM were markedly suppressed after treatment with SAM (a DNA methylation agent), resulting in extensive *BLM* promoter methylation. DLD1 cells failed to remethylate on exposure to *S*-adenosyl-*l*-homocysteine (an unmethylated analogue) used as a control. SAM treatment caused a marked accumulation of DNA damage foci and G_2 arrest in DLD1 cells (data not shown). Instead, remethylation on SAM exposure did not affect *BLM* expression in HT29 cells as indicated by Western blot analysis. Consistently, SAM led to a significant time-dependent decrease of the proliferation rate in DLD1 cells but not in HT29 cells ($P = 0.001$; Fig. 4d). The repression of *BLM* on SAM treatment was also observed in RKO and HCT116 cells (data not shown). Taken together, these data suggest that epigenetic modification through promoter hypomethylation may contribute to the increased *BLM* expression and hypersensitivity to DNA damage agents in CRC.

Increased levels of *BLM* contribute to poor tumor differentiation and hypersensitivity to DNA-damaging agents

We reasoned that DLD1 cells as being unmethylated and overexpressing *BLM* could be a good model to examine the effects of *BLM* knockdown on the cellular phenotype and response to DNA-damaging agents. Therefore, DLD1 cells were transfected with a pool of three short hairpin RNAs targeting the *BLM* gene and a control vector. After selection, we observed a consistent depletion of BLM to 2.8-fold lower then in DLD1 cells transfected with the control vector (Fig. S8b). Knockdown of *BLM* resulted in a significant upregulation of the differentiation markers cytokeratin 20 and retinoic acid receptor β and reduced vimentin expression as compared with the controls by Western blot analysis (Fig. S8b). Loss of *BLM* expression led to the appearance of cell aggregates containing densely packed round cells and faint basophilic stain not observable in the control cells. These latter were characterized by elongated tumor cells with cytosolic processes and basophilic stain mirroring a fibroblast-like phenotype (Fig. S8b). In addition, *BLM* silencing abolished hypersensitivity to the methylating agent SAM as compared with control cells but did not interfere significantly with 5-aza-2′-deoxycytidine activity (Fig. S8c, d and data not shown). Forced overexpression of *BLM* in HT29 cells induced cellular dedifferentiation and enhanced sensitivity to the methylating agent SAM (data not shown). Taken together, these findings suggest that increased levels of *BLM* might promote poor differentiation of the tumor and increased sensitivity to DNA methylating agents in distinct cellular subtypes.

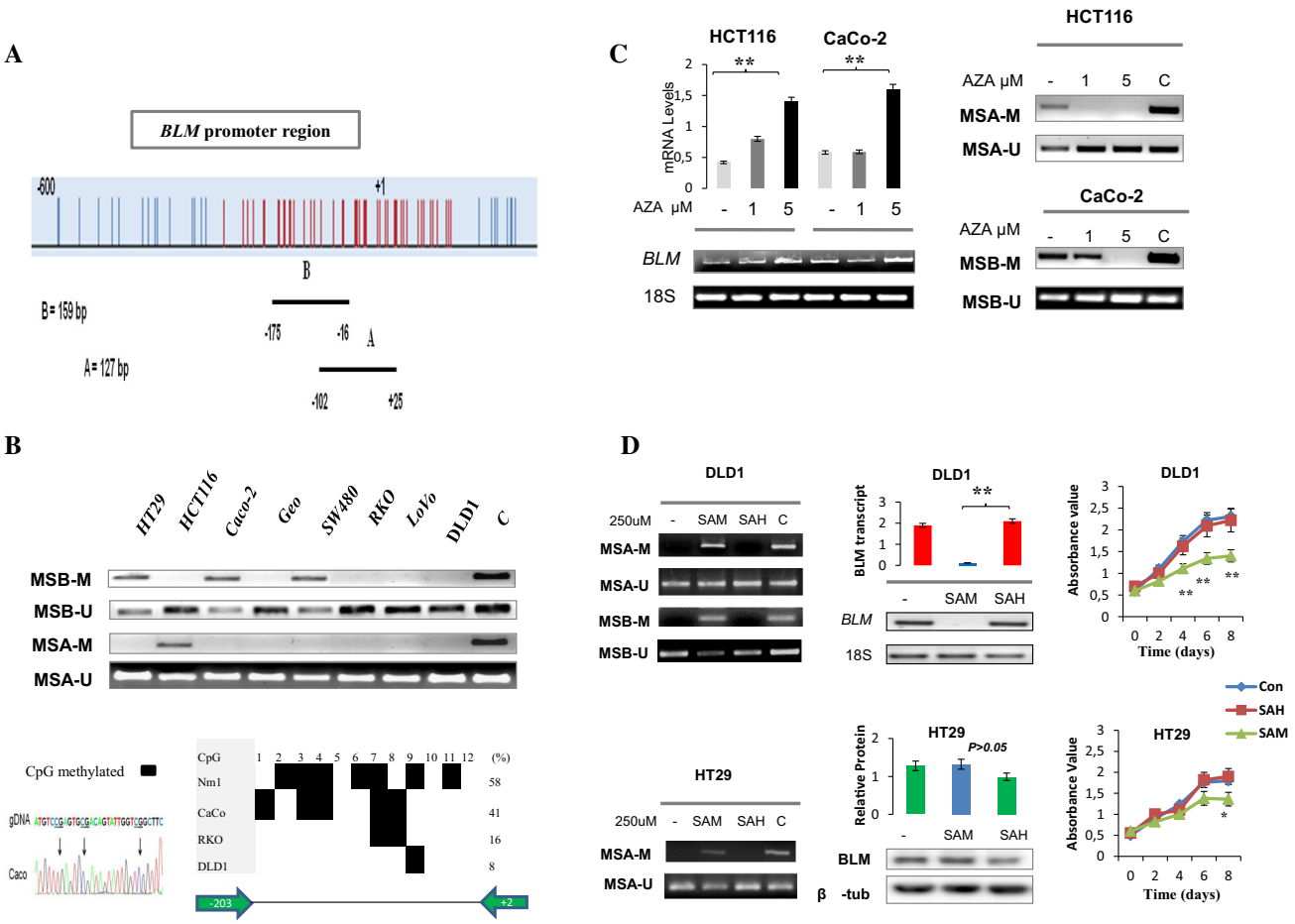

Fig. 4 *BLM* CpG island promoter hypomethylation leads its overexpression in human colorectal cancer (CRC) cell lines. **a** The CpG island (*red area*) encompassing the transcription start site of the *BLM* promoter region. CpG dinucleotides are represented as *short vertical lines*, whereas the position of the methylation-specific PCR regions—A (*MSA*) (−102 to +25) and B (*MSB*) (−175 −16)— is evidenced by *two horizontal lines*. **b** Methylation-specific PCR for the *BLM* gene in CRC-derived cell lines. The presence of a PCR band under *lane M* or *lane U* indicates methylated or unmethylated forms respectively. Bisulfite genomic sequencing data in representative CRC cell lines compared with normal colon (*Nm1*), "normal appearing colonic mucosa taken from a healthy control," are shown along with the percentage of methylated CpG residues for each sample. The chromatogram (on the *left*) after bisulfite sequencing shows two of three CpG dinucleotides (*black arrows*) methylated in CaCo-2 cells. Methylated cytosine is indicated by a *black square*. **c** Treatment with the demethylating agent 5-aza-2′-deoxycytidine (*AZA*; 5uM) increases *BLM* gene expression (quantitative reverse transcription PCR) and causes loss of the methylated bands in both promoter regions in the cell lines indicated. $^{**}P \leq 0.01$ by a two-tailed *t* test. **d** Treatment with *S*-adenosyl-L-methionine (*SAM*), but not with *S*-adenosyl-*l*-homocysteine (*SAH*), its unmethylated analogue control, induces methylation at the *BLM* promoter in fully unmethylated DLD1 cells by methylation-specific PCR. Consequently, *BLM* messenger RNA (*mRNA*) expression decreases in SAM-treated cells or remains unchanged in SAH-treated cells. By contrast, SAM-treated HT29 cells become partially methylated, resulting in unchanged BLM expression levels compared with controls by Western blot. $P > 0.05$ by a two-tailed *t* test. The cell proliferation rate is significantly lower in unmethylated DLD1 ceels than in methylated HT29 cells on SAM treatment as compared with SAH-treated control groups. $^{*}P \leq 0.05$, $^{**}P \leq 0.01$ by a two-tailed *t* test. PCR products were run on a 2 % agarose gel and for each methylation-specific PCR experiment either an unmethylated or an in vitro methylated DNA positive control was used. They are indicated by *C*. Data are presented as the mean ± standard deviation of three independent experiments. *gDNA* genomic DNA, *M* methylated products, *β-tub* β-tubulin, *U* unmethylated products

Epigenetic-associated overexpression and BLM cytoplasmic mislocalization predicts good clinical response to DNA-damaging agents in CRC patients

We assessed the prevalence of *BLM* CpG island promoter methylation in clinical cancer specimens by using our subgroup of CRCs and paired normal mucosa. In nonneoplastic samples compared with paired CRC samples, the frequency of methylated region A was not statistically different (30 %, 25 of 82, vs 33 %, 27 of 82). In contrast, the frequency of methylated region B was significantly higher in normal mucosa than in matched CRC samppls, mirroring in vitro CRC cell lines (100 %, 82 of 82, vs 34 %, 28 of 82; $P = 0.0003$;

Fig. S6c). Notably, 40 % of tumors were unmethylated in both region A and region B and associated with increased *BLM* expression levels in primary tumors, poor differentiation, and advanced tumor stage (III/IV), suggesting that *BLM* undergoes hypomethylation-associated overexpression even in clinical CRCs specimens (Fig. S6d). Moreover, we observed reproducible rates of *BLM* locus-specific downmethylation in tumors versus normal paired samples by genomic DNA methylation patterns and bisulfite sequencing analysis (Fig. S7c, d). To further investigate the effects of cytoplasmic accumulation of BLM and DDR on CRC progression, we screened a training cohort of TMAs comprising 130 CRCs and 60 matched normal tissues. BLM immunostaining was always positive and mostly confined to the nucleus in the normal colonic epithelial and surrounding stromal cells (Fig. 5a). CRC specimens frequently exhibited a higher percentage of BLM-positive cells and a distinct localization between the cytoplasm and the nucleus compared with normal controls, supporting the in vitro findings (Fig. 5a). We then classified the BLM subcellular distribution pattern into three categories: nuclear (30 %; 39 of 130), nuclear/cytoplasmic (26 %; 31 of 130), and cytoplasmic (44 %, 60 of 130). Nuclear expression of BLM was more common in fully methylated *BLM* tumors than in those with nuclear/cytoplasmic or cytoplasmic positivity, suggesting that hypomethylation is associated with an altered BLM expression pattern (Figs. 5a, S7d). Intriguingly, we observed that tumors with high *BLM* mRNA expression, lymph node metastasis, and diffuse staining for pATM and γH2AX exhibited a high level of cytoplasmic expression of BLM ($P < 0.01$; Fig. 5b, c). We next assessed the prognostic impact of the BLM subcellular mislocalization. Kaplan–Meier curve analysis indicated a mild but significant association between cytosolic BLM and decreased overall survival; however, the significance was not maintained in multivariate analysis ($P = 0.037$; Fig. 5d and data not shown). To further investigate the potential relationship between BLM and clinical response to the DNA-damaging agents, we examined BLM subcellular expression in metastatic CRC patients treated with irinotecan, a topoisomerase inhibitor that induces DNA damage and formation of double-strand breaks [10]. Cytoplasmic expression of BLM was a significant predictor of long-term progression-free survival compared with the BLM nuclear distribution pattern (adjusted HR 1.89; 95 % CI 1.10–3.24; $P = 0.021$; Fig. 5d). These data suggest that epigenetic mechanisms as well as BLM cytosolic accumulation may be relevant for its appropriate DNA repair function and hence hypersensitivity to DNA-damaging agents in patients.

Discussion

Dysregulation of DNA damage repair plays a fundamental role in carcinogenesis, affecting responses to DNA-damaging anticancer therapy. DNA damage occurs through exposure to external toxic agents (e.g., irradiation, genotoxic chemicals, inflammatory cytokines, or hypoxia) and more frequently by errors produced during DNA replication [8–12]. Germline or somatic mutations of the DDR genes are common in many types of human cancers, underlying that genomic stability is crucial to prevent human diseases [10]. In the context of CRC, the most known cause of DNA repair defects involves the loss a series of tumor suppressor genes (*MLH1*, *MSH2*, *MSH6*, *MBD4*, *WRN*) implicated in several DNA repair pathways: mismatch repair, base excision repair, or homologous recombinational repair [10, 14]. Recently it has been suggested that increased levels of DDR and mutations in the ATM signaling may be of help in identifying tumors that are susceptible to specific therapeutic agents [24–27]. Defects in RecQ helicase homologue protein, as well as molecular mechanisms underlying genome-wide DNA damage, have been little explored in sporadic neoplasms thus far.

Here we have demonstrated that BLM, a central player of the RecQ helicase family, undergoes epigenetic upregulation by CpG island promoter hypomethylation and aberrant cytoplasmic localization in CRC cells. Overexpression of the RecQ helicases as predictive biomarkers of clinical response to certain chemotherapeutic agents has recently been reported in colon cancer [25–27]. Despite the proved role of BLM as a tumor suppressor gene both in Bloom syndrome and in a mouse model of intestinal cancer, we observed overexpression of BLM in primary CRCs [8]. Our observations in independent data sets suggest that *BLM* is closely related to an activated ATM signaling, supporting the hypothesis that these pathways may be mostly deregulated in response to genotoxic and exogenous insults, generated during carcinogenesis and consistent with increased levels of DNA lesions.

We found that elevated expression levels of *BLM* are related to cytoplasmatic accumulation and formation of DNA-damage-induced foci, likely resulting in the formation of the so-called cytoplasmic foci and molecular distinct subgroups displaying a CIMP and poorly differentiated phenotype [28]. Indeed, large-scale analysis of DNA-damaging agents has revealed global changes of repair proteins into discrete subcellular clusters or foci, underlying a constitutive activation of the DDR pathway, which may represent a triggering factor in promoting carcinogenesis [28, 29]. Consistent with this model, it has been proposed that defects in BLM modification by small

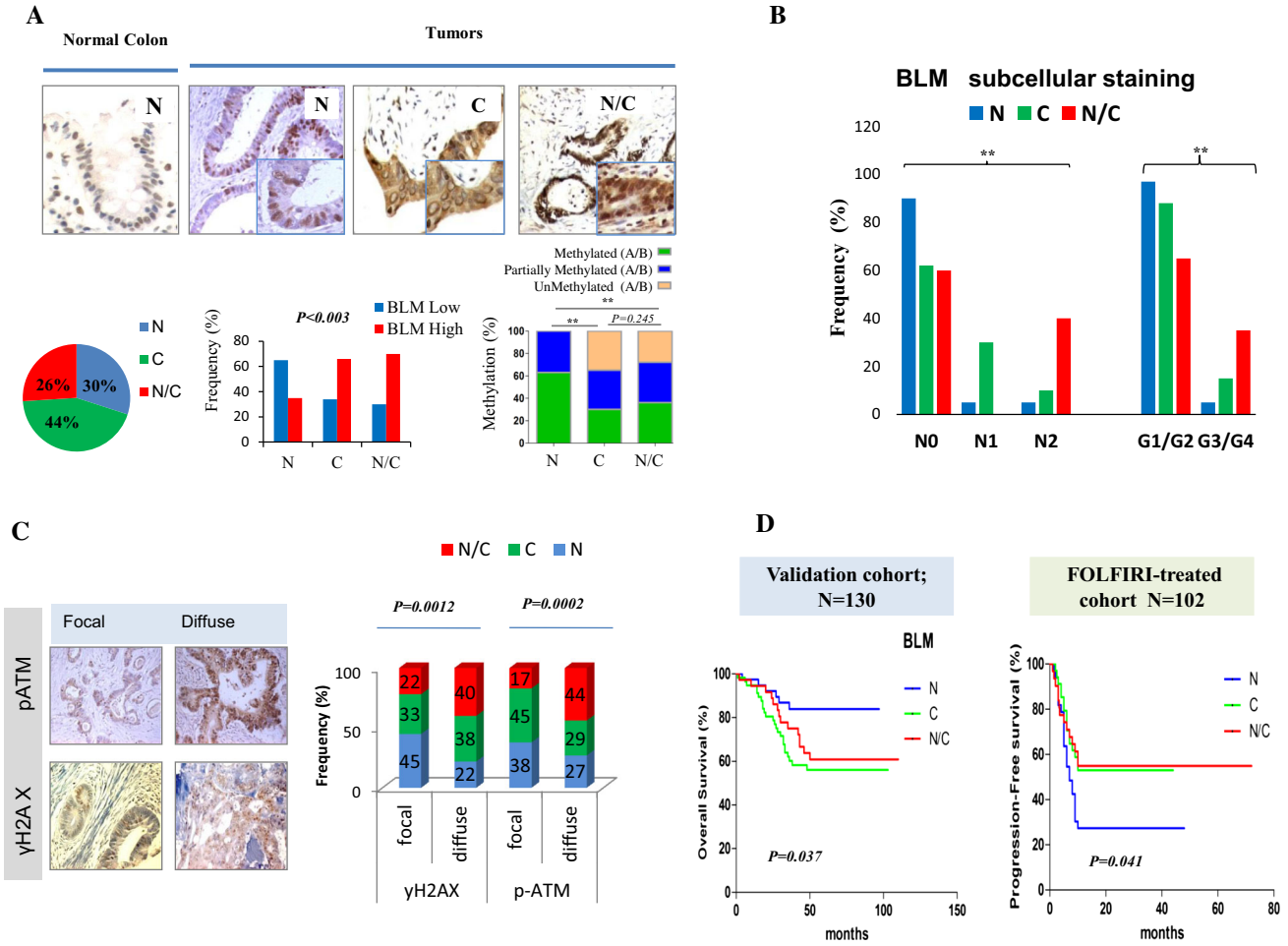

Fig. 5 Clinical significance of BLM expression and DNA damage response in colorectal cancer specimens. **a** Representative examples of tissue microarray histologic sections showing BLM staining and its cellular distribution in normal colonic mucosa and tumors. BLM subcellular distribution is correlated to transcript levels (messenger RNA) or methylation status in the validation cohort of primary colorectal cancer (CRC) specimens ($N = 82$). $^{*}P \leq 0.05$, $^{**}P \leq 0.01$ by the chi-square test. **b** BLM expression pattern in relation to lymph node metastases (*N0* absence, *N1* positivity in up to three lymph nodes, *N2* positivity in four or more lymph nodes) and tumor differentiation (*G1/G2* low or moderate grade, *G3/G4* high or very high grade). $^{**}P \leq 0.01$ by the chi-square test. **c** The level of DNA damage response, positive staining (focal or diffuse) for γH2AX and phosphorylated ataxia telangiectasia mutated (*p-ATM*) in the tumor specimens, is related to BLM subcellular distribution. *P* was obtained by the chi-square test. **d** Cytoplasmic expression of BLM is associated with shorter overall survival compared with BLM nuclear expression in the validation cohort ($N = 130$) of stage I-IV CRC. *P* was obtained by the log-rank test. Cytoplasmic BLM localization predicts a longer progression-free survival in patients receiving a 5-fluorouracil, irinotecan, and leucovorin (*FOLFIRI*) chemotherapy regime in an independent data set ($n = 102$) of metastatic CRCs. *P* was obtained by the log-rank test. *C* cytoplasmic expression, *N* prevalent nuclear expression, *N/C* nuclear and cytoplasmic expression

ubiquitin-related modifier (SUMO) proteins can cause increased levels of γH2AX foci. Thus, SUMOylation might also be important in mediating the localization of BLM to nuclear bodies in damaged cells. Although SUMO genes are highly correlated with BLM-overexpressing tumors, their impact on tumor progression remains to be established [29].

Genome-wide DNA hypomethylation is a frequent epigenetic alteration in CRC and has been associated with the activation of certain proto-oncogenes and the presence of chromosomal instability [30, 31]. By dissecting the *BLM* proximal promoter, we have demonstrated that loss of methylation of a specific promoter region increases *BLM* transcript expression, implying that its overexpression is triggered, at least partially, by DNA hypomethylation in certain molecular subtypes preferentially displaying CIMP or chromosomal instability. Supporting this idea, 5-aza-2′-deoxycytidine treatment abolished promoter methylation and induced overexpression of *BLM* in methylated non-CIMP cancer cell lines. SAM treatment instead reversed promoter hypomethylation and reduced *BLM* transcript expression in more invasive CIMP cancer cells. In DKO

cells, maintenance of methylation is lost and *BLM* is upregulated, suggesting that DNA methylation is important to suppress the expression at the *BLM* promoter. In addition, loss of function experiment has provided further insight into the BLM's contribution to the tumorigenic process.

In recent decades, CpG island hypermethylation has been considered the predominant mechanism leading to inactivation of DNA repair genes in sporadic CRC [11, 14]. Globally, our data provide the first evidence that DNA hypomethylation can activate key DNA repair genes, thus influencing the levels of DDR as an additional mechanism to increase genome instability. This supports the hypothesis that DNA demethylation and CpG island hypermethylation may be partially overlapped in certain molecular subtypes [11, 14].

The clinical relevance of deregulated BLM expression and DDR was validated in our data sets. We showed that the *BLM* promoter is methylated in normal mucosa and becomes hypomethylated in a significant proportion of primary tumors. Accordingly, BLM is markedly expressed in poorly differentiated CRCs and its predominant localization in cytoplasm reflects consistent DDR in tumor tissues, providing support to in vitro findings. Indeed, cytoplasmic expression of BLM is accompanied by accumulation of unpaired DNA damage (increased staining for pATM and γH2AX) and decreased overall survival. Remarkably, we were able to demonstrate that cytoplasmic BLM accumulation renders metastatic CRC very sensitive to the action of inhibitors of topoisomerase and DNA-damaging agents. These observations suggest a role of BLM dysfunction in the development of recurrence. In support of our findings, previous studies have indicated that other homologous recombination (HR) DNA repair genes such as *BRCA1* or poly(ADP-ribose) polymerase PARP genes, can be mislocalized in the cytosol [32, 33]. Notably, cytoplasmic expression of BRCA1 or PARP correlates with an unfavorable long-term prognosis and high sensitivity to neoadjuvant-based chemotherapy in breast cancer [32, 33].

In summary, our results suggest a scenario whereby epigenetic deregulation of caretaker DNA repair genes and their dislocation in the cytoplasm contribute to damaging the integrity of the genome in cancer cells. In addition to the well-known mechanisms of epigenetic silencing of *MLH1*, our results highlight for the first time that promoter DNA hypomethylation and protein subcellular localization may reflect distinct levels of BLM repair capacity in CRC. Although this study is suggestive of an association between cytosolic BLM and colon cancer progression, additional investigation is warranted to further define the mechanisms by which cytosolic BLM influences metastasis.

The novel relationship between BLM and increased risk of CRC progression during therapy may be of value to identify patients who are susceptible to specific chemotherapeutic agents.

Acknowledgments Part of this study was funded by the Italian Ministry of University and Research (MiUR) through a grant to Massimo Pancione. We would like to thank all the scientists who have contributed through their valuable advice to this article's production.

Compliance with ethical standards

Conflict of interest The authors declare that they have no conflict of interest.

Funding Part of this study was funded by the FUR and the Italian Ministry of University and Research (MiUR) by grants to Massimo Pancione.

References

1. Negrini S, Gorgoulis VG, Halazonetis TD. Genomic instability an evolving hallmark of cancer. Nat Rev Mol Cell Biol. 2010;11:220–8.
2. Pancione M, Remo A, Colantuoni V. Genetic and epigenetic events generate multiple pathways in colorectal cancer progression. Pathol Res Int. 2012;2012:509348.
3. Remo A, Pancione M, Zanella C, et al. Molecular pathology of colorectal carcinoma. A systematic review centered on the new role of pathologist. Pathologica. 2012;104:432–41.
4. Gruber SB, Ellis NA, Scott KK, et al. BLM heterozygosity and the risk of colorectal cancer. Science. 2002;297:2013–4.
5. Wu L, Hickson ID. The Bloom's syndrome helicase suppresses crossing over during homologous recombination. Nature. 2003;426:870–4.
6. Chu WK, Hickson ID. RecQ helicases: multifunctional genome caretakers. Nat Rev Cancer. 2009;9:644–54.
7. Pino MS, Chung DC. The chromosomal instability pathway in colon cancer. Gastroenterology. 2010;138:2059–72.
8. Traverso G, Bettegowda C, Kraus J, et al. High recombination and genetic instability in BLM-deficient epithelial cells. Cancer Res. 2003;63:8578–81.
9. Burrell RA, McClelland SE, Endesfelder D, et al. Replication stress links structural and numerical cancer chromosomal instability. Nature. 2013;494:492–6.
10. Lord CJ, Ashworth A. The DNA damage response and cancer therapy. Nature. 2012;48:287–94.
11. Potenski CJ, Klein HL. The expanding arena of DNA repair. Nature. 2011;471:48–9.
12. Beckman RA, Loeb LA. Genetic instability in cancer: theory and experiment. Semin Cancer Biol. 2005;15:423–35.
13. Stephens PJ, Greenman CD, Fu B, et al. Massive genomic rearrangement acquired in a single catastrophic event during cancer development. Cell. 2011;144:27–40.
14. Lahtz C, Pfeifer GP. Epigenetic changes of DNA repair genes in cancer. J Mol Cell Biol. 2011;3:51–8.
15. Cancer Genome Atlas Network. Comprehensive molecular characterization of human colon and rectal cancer. Nature. 2012;487:330–7.
16. Sheffer M, Bacolod MD, Zuk O, Giardina SF, Pincas H, Barany F, et al. Association of survival and disease progression with chromosomal instability: a genomic exploration of colorectal cancer. Proc Natl Acad Sci U S A. 2009;106:7131–6.
17. Smith JJ, Deane NG, Wu F, et al. Experimentally derived metastasis gene expression profile predicts recurrence and death

in patients with colon cancer. Gastroenterology. 2010;138:958–68.
18. Barretina J, Caponigro G, Stransky N, et al. The Cancer Cell Line Encyclopedia enables predictive modelling of anticancer drug sensitivity. Nature. 2012;483(7391):603–7.
19. Pancione M, Remo A, Zanella C, et al. The chromatin remodelling component SMARCB1/INI1 influences the metastatic behavior of colorectal cancer through a gene signature mapping to chromosome 22. J Transl Med. 2013;11:297.
20. Pagnotta SM, Laudanna C, Pancione M, et al. Ensemble of gene signatures identifies novel biomarkers in colorectal cancer activated through PPARγ and TNFα signaling. PLoS One. 2013;8:e72638.
21. Takabayashi H, Wakai T, Ajioka Y, et al. Alteration of the DNA damage response in colorectal tumor progression. Hum Pathol. 2013;44:1038–46.
22. Simmer F, Brinkman AB, Assenov Y, et al. Comparative genome-wide DNA methylation analysis of colorectal tumor and matched normal tissues. Epigenetics. 2012;7:1355–67.
23. Pancione M, Sabatino L, Fucci A, et al. Epigenetic silencing of peroxisome proliferator-activated receptor γ is a biomarker for colorectal cancer progression and adverse patients' outcome. PLoS One. 2010;5:e14229.
24. Khalil HS, Tummala H, Chakarov S, et al. Targeting ATM pathway for therapeutic intervention in cancer. Biodiscovery. 2012;1:3.
25. Lao VV, Welcsh P, Luo Y, et al. Altered RECQ helicase expression in sporadic primary colorectal cancers. Transl Oncol. 2013;6:458–69.
26. Brosh RM Jr. DNA helicases involved in DNA repair and their roles in cancer. Nat Rev Cancer. 2013;13:542–58.
27. Sharma S. An appraisal of RECQ1 expression in cancer progression. Front Genet. 2014;5:426.
28. Tkach JM, Yimit A, Lee AY, et al. Dissecting DNA damage response pathways by analysing protein localization and abundance changes during DNA replication stress. Nat Cell Biol. 2012;14:966–76.
29. Bergink S, Jentsch S. Principles of ubiquitin and SUMO modifications in DNA repair. Nature. 2009;458:461–7.
30. Hoffmann MJ, Schulz WA. Causes and consequences of DNA hypomethylation in human cancer. Biochem Cell Biol. 2005;83:296–321.
31. Suzuki K, Suzuki I, Leodolter A, et al. Global DNA demethylation in gastrointestinal cancer is age dependent and precedes genomic damage. Cancer Cell. 2006;9:199–207.
32. Jiang J, Yang ES, Jiang G, et al. p53-dependent BRCA1 nuclear export controls cellular susceptibility to DNA damage. Cancer Res. 2011;71:5546–57.
33. von Minckwitz G, Müller BM, Loibl S, et al. Cytoplasmic poly(adenosine diphosphate-ribose) polymerase expression is predictive and prognostic in patients with breast cancer treated with neoadjuvant chemotherapy. J Clin Oncol. 2011;29:2150–7.